Mon. Not. R. Astron. Soc. **000**, 000–000 (0000) Printed 1 February 2008 (MN LATEX style file v1.4)

A Survey of hard spectrum *ROSAT* sources 2: optical identification of hard sources

M.J. Page[1], J.P.D. Mittaz[1], F.J. Carrera[1,2]

[1] *Mullard Space Science Laboratory, University College London, Holmbury St Mary, Dorking, Surrey RH5 6NT, UK.*

[2] *Instituto de Física de Cantabria (Consejo Superior de Investigaciones Científicas–Universidad de Cantabria), 39005 Santander, Spain.*

ABSTRACT

We have surveyed 188 *ROSAT* PSPC fields for X–ray sources with hard spectra ($\alpha < 0.5$); such sources must be major contributors to the X–ray background at faint fluxes. In this paper we present optical identifications for 62 of these sources: 28 AGN which show broad lines in their optical spectra (BLAGN), 13 narrow emission line galaxies (NELGs), 5 galaxies with no visible emission lines, 8 clusters and 8 Galactic stars.

The BLAGN, NELGs and galaxies have similar distributions of X–ray flux and spectra. Their *ROSAT* spectra are consistent with their being AGN obscured by columns of $20.5 < \log(N_H/\mathrm{cm}^{-2}) < 23$. The hard spectrum BLAGN have a distribution of X–ray to optical ratios which is similar to that found for AGN from soft X–ray surveys ($1 < \alpha_{OX} < 2$). However, a relatively large proportion (15%) of the BLAGN, NELGs and galaxies are radio loud. This could be because the radio jets in these objects produce intrinsically hard X–ray emission, or if their hardness is due to absorption, it could be because radio loud objects are more X–ray luminous than radio quiet objects. The 8 hard sources identified as clusters of galaxies are the brightest, and softest group of sources and hence clusters are unlikely to be an important component of the hard, faint population.

We propose that BLAGN are likely to constitute a significant fraction of the faint, hard, 0.5 - 2 keV population and could be important to reproducing the shape of the X–ray background, because they are the most numerous type of object in our sample (comprising almost half the identified sources), and because all our high redshift ($z > 1$) identified hard sources have broad lines.

1 INTRODUCTION

The origin of most of the X–ray emission in the Universe is still unknown because the sources that produce most of the > 2 keV X–ray background (XRB) are still to be resolved. *ROSAT* surveys have succeeded in resolving $\sim 80\%$ of the 1-2 keV XRB into individual sources (Hasinger et al. 1998), and optical identification and X–ray spectroscopy has been possible for brighter sources which produce $\sim 40\%$ of the 1-2 keV background. The majority of these sources are broad line AGN (hereafter BLAGN), and at faint fluxes narrow emission line galaxies (hereafter NELGs, McHardy et al. 1998); Schmidt et al. (1998) argued that the NELGs are also AGN, but with low luminosity or obscured broad line regions. On average, faint NELGs have harder X–ray spectra ($f_\nu \propto \nu^{-\alpha}$ with $\alpha \sim 0.5$, Romero-Colmenero et al. 1996, Almaini et al. 1996) than the broad line AGN which have mean $\alpha \sim 1$ (Mittaz et al. 1999, Ciliegi et al. 1994).

Despite the success of *ROSAT* surveys, the XRB cannot be synthesised by extrapolating the observed source populations to faint fluxes, because the resultant spectrum would be softer than that of the background; this discrepancy is present for all energy bands between 0.5 and 40 keV. This means that at faint fluxes there must be a population of sources with spectra that are harder than the background. According to leading models, these hard sources (eg Fabian 1999, Gilli, Risaliti & Salvati 1999) are obscured AGN. However, the physical nature and observational appearance of the XRB producing population is not yet known, and is the subject of some debate. For example, Gilli, Risaliti & Salvati (1999) examined a model intended to reproduce the XRB by extrapolating the X–ray emission of present epoch AGN to high redshift using the observed soft X–ray luminosity function. In contrast, the model of Fabian (1999) has a large fraction of the XRB due to a population of high redshift, heavily obscured, growing AGN, which are different to anything observed in the local universe.

In Page et al. (2000), hereafter paper 1, we presented a catalogue of 147 serendipitous *ROSAT* sources which have spectra harder than that of the XRB. These sources have a steep $N(S)$ relation down to the sensitivity limit of our survey ($\sim 10^{-14}$ erg cm^{-2} s^{-1}), and are therefore likely to be the bright tail of the population of hard sources that

dominate the source counts at faint fluxes. As such, they could offer us a preview of the faint, hard and dominant, X-ray source population. We have therefore undertaken a programme of optical and infrared observations of our *ROSAT* hard source sample to find out what these sources are. In this paper we present the hard source identifications obtained from our optical (spectroscopic) campaign together with those found in existing catalogues. Section 2 details our method and observations, the results of which are given in Section 3. These results are discussed in the context of absorbed AGN and the XRB in Section 4. Finally, we present our conclusions in Section 5.

Throughout this paper we define power law spectral index α such that $f_\nu \propto \nu^{-\alpha}$.

2 OPTICAL IDENTIFICATION

2.1 Strategy

To produce a systematic and efficient optical identification programme, we divided the hard X-ray sources into two groups depending on the ease of optical identification. Sources which had one or two plausible candidates present in APM data and/or the DSS were considered suitable for optical spectroscopy and make up the 'spectroscopic sample', while sources with no plausible candidates, or more than two, were considered unsuitable for spectroscopy and became the 'imaging sample'. There are 103 sources in the spectroscopic sample and 44 sources in the imaging sample. This paper will deal only with identified sources from the spectroscopic sample (except for two sources, RXJ005812.20-274217.8 and RXJ101112.05+554451.3, which are fainter than our spectroscopic sample limit but have catalogue identifications). The properties of sources in the imaging sample, and their relationship to the spectroscopic sample sources, will be discussed briefly in Section 3.2 and in more detail in Carrera et al. (in preparation) where we will present the results of our optical and infrared imaging. The three sources of data for the identification process were spectra taken on the William Herschel Telescope (WHT) and the European Southern Observatory 3.6m Telescope (ESO 3.6), and databases of existing catalogues. The optical spectra will be presented in Mittaz et al. (2001) along with a full description of the observations and data reduction.

Catalogue identifications were obtained by searching the NASA Extragalactic Database (NED) and SIMBAD around all the *ROSAT* hard source positions (not just the spectroscopic sample). One further source (RXJ043420.48-082136.7) was identified from a WHT ISIS spectrum taken during the RIXOS programme, but was not part of the final RIXOS sample presented in Mason et al. (2000).

3 RESULTS

Table 1 contains the list of optical identifications. We have categorised our sources as follows. X-ray sources with an optical counterpart which is a Galactic star, of any type, have been classified as stars, and X-ray sources which are clusters of galaxies have been classified as clusters. X-ray sources with an extragalactic optical counterpart which has one or more broad emission lines, or a broad component (> 2000 km s^{-1}) to an emission line, is classified as a broad line AGN (BLAGN). X-ray sources with galaxy optical counterparts showing narrow emission lines (< 2000 km s^{-1}) but no broad emission lines are classed as narrow emission line galaxies (NELGs). Note that none of the narrow line objects in this survey would be classified as narrow line Seyfert 1s (eg by the criteria given in Goodrich 1989). Galaxies with no discernable emission lines were classed as galaxies. The numbers of objects in each category, and their mean properties are given in Table 2. The sample is dominated by extragalactic sources, and of these over half are broad line AGN.

Table 2. Different types of identified hard sources and their mean properties. N is the number of sources, $\langle S \rangle$ is the mean fitted flux in units of 10^{-14} erg cm^{-2} s^{-1}, $\langle \alpha \rangle$ is the mean fitted spectral slope, $\langle z \rangle$ is the mean redshift and $\langle \log\ L \rangle$ is the mean of the log of observed 0.5 - 2 keV luminosity in erg s^{-1}, calculated as described in Section 3.3. For comparison, the unidentified sources from the spectroscopic sample are listed as No ID (S), while the unidentified sources from the imaging sample are listed as 'No ID (I)'.

	N	$\langle S \rangle$	$\langle \alpha \rangle$	$\langle z \rangle$	$\langle \log\ L \rangle$	$\langle offset \rangle$
BLAGN	28	8.1	-0.29	1.00	43.71	6.1
NELGs	13	13.6	-0.74	0.25	42.68	7.2
galaxies	5	4.0	-0.43	0.12	41.85	6.5
clusters	8	19.9	0.21	0.23	43.38	-
stars	8	3.1	-0.91	-	-	11.45
No ID (S)	43	3.9	-0.52	-	-	-
No ID (I)	42	3.2	-0.54	-	-	-

The distributions of offsets between the X-ray positions and the optical counterparts for the different classes of hard source are shown in Fig. 1. The mean offsets for each source type are given in Table 2 and are $6 - 7$ arcseconds for all source types except for the Galactic stars, which have a mean offset of 12 arcseconds and a flat distribution of offsets (Fig. 1); this suggests that the 'star' identifications are less secure than the others.

We have systematically checked the redshifts of the extragalactic hard sources for similarity to the redshifts of the targets of the PSPC observations in which they were detected. Only two sources, RXJ111926.34+210646.1 and RXJ120403.79+280711.2, both clusters of galaxies, have redshifts similar to the observation targets.

3.1 X-ray slopes and fluxes

The fitted X-ray spectral slopes and fluxes of the different types of sources are shown in Fig. 2, and their mean slopes and fluxes are given in Table 2. A noticeable feature of Fig. 2 is that the clusters of galaxies are concentrated towards the top right (soft spectrum, high flux) corner compared to the other sources. This trend is confirmed by a two dimensional Kolmogorov Smirnov (2DKS) test (Fasano & Franceschini 1987): the cluster distribution of (α, S) is different to that for any (or all) of the other source types with $> 99\%$ confidence. Because they are not particularly hard, and because they are predominantly bright and therefore do not have as steep an $N(S)$ relation as the rest of the hard sources, the clusters are unlikely to be important contributors to the faint hard source population.

Table 1. Hard source optical counterparts

Source	optical position RA	dec	origin	type	z	cat name	notes
RXJ001144.43-362638.0	00 11 44.54	-36 26 39.0	EFOSC	BLAGN	0.900		
RXJ004651.98-204329.0	00 46 51.83	-20 43 28.6	cat	BLAGN	0.380	[HB89] 0044-209	
RXJ005734.78-272827.4	00 57 34.94	-27 28 28.0	EFOSC	BLAGN	2.185		
RXJ005736.81-273305.9	00 57 36.75	-27 33 04.6	cat	NELG	0.213	GSGP 4X:069	
RXJ005746.75-273000.8	00 57 46.83	-27 30 00.9	cat	galaxy	0.019	ESO 411- G 034	
RXJ005801.64-275308.6	00 58 01.32	-27 53 10.2	EFOSC	NELG	0.416	GSGP 4X:091	
RXJ005812.20-274217.8	00 58 13.57	-27 42 11.4	cat	NELG	0.597	GSGP 4X:100	
RXJ013555.47-183210.2	01 35 55.71	-18 32 24.9	EFOSC	star	0.000		
RXJ013707.63-183846.4	01 37 07.75	-18 38 49.9	EFOSC	star	0.000		Unlikely to be X-ray source
RXJ013721.47-182558.3	01 37 21.94	-18 26 03.0	EFOSC	NELG	0.336		
RXJ014159.22-543037.0	01 41 59.81	-54 30 39.6	EFOSC	BLAGN	0.168		
RXJ031456.58-552006.8	03 14 56.30	-55 20 06.1	cat	galaxy	0.387	[GZd97] 1.4GHz 38	
RXJ033340.22-391833.4	03 33 39.54	-39 18 41.4	EFOSC	BLAGN	1.436		
RXJ033402.54-390048.7	03 34 03.26	-39 00 36.9	EFOSC	galaxy	0.061	PKS 0332-39	WAT radio source
RXJ034119.02-441033.3	03 41 19.23	-44 10 29.9	cat	BLAGN	0.505	QSF3X:51	
RXJ043420.48-082136.7	04 34 20.19	-08 21 31.3	cat	BLAGN	0.155		
RXJ045558.99-753229.1	04 55 58.82	-75 32 28.0	cat	NELG	0.018	ESO 033- G 002	
RXJ052839.93-325148.5	05 28 39.83	-32 51 44.7	cat	cluster	0.273	[VMF98] 042	
RXJ082640.20+263112.3	08 26 40.52	+26 31 14.1	ISIS	NELG	0.182		
RXJ085340.52+134924.9	08 53 41.01	+13 49 19.7	cat	NELG	0.190	MS 0850.8+1401	Uncertain ID
RXJ085851.49+141150.7	08 58 50.75	+14 11 54.5	ISIS	NELG	0.453		
RXJ090518.27+335006.0	09 05 17.94	-33 50 16.1	ISIS	NELG	0.425		
RXJ090923.64+423629.2	09 09 23.82	+42 36 23.3	ISIS	BLAGN	0.177		
RXJ091908.27+745305.6	09 19 10.56	+74 53 11.2	ISIS	galaxy	0.073		
RXJ094144.51+385434.8	09 41 44.61	+38 54 39.1	ISIS	BLAGN	1.819		
RXJ095340.67+074426.1	09 53 40.12	+07 44 12.3	cat	BLAGN	0.760	RIXOS F218_021	Uncertain ID
RXJ101008.53+513334.9	10 10 08.91	+51 33 31.0	ISIS	star	0.000		
RXJ101112.05+554451.3	10 11 12.30	+55 44 47.0	cat	BLAGN	1.246	87GB 100755.1+560014	
RXJ101123.17+524912.4	10 11 22.67	+52 49 12.3	ISIS	BLAGN	1.012		
RXJ101147.48+505002.2	10 11 47.82	+50 49 57.5	ISIS	BLAGN	0.079	5H 23	
RXJ104648.27+541235.4	10 46 48.88	+54 12 19.4	ISIS	star	0.000		
RXJ104723.37+540412.6	10 47 23.50	+54 04 06.7	ISIS	BLAGN	1.500		
RXJ110742.05+723236.0	11 07 41.59	+72 32 35.8	cat	BLAGN	2.100	[HB89] 1104+728	
RXJ111750.51+075712.8	11 17 50.78	+07 57 11.4	cat	BLAGN	0.698	RIXOS F258_001	
RXJ111926.34+210646.1	11 19 25.93	+21 06 47.4	cat	cluster	0.176		
RXJ111942.16+211518.1	11 19 42.13	+21 15 16.6	cat	BLAGN	1.288		
RXJ112056.87+132726.2	11 20 57.48	+13 27 08.0	ISIS	star	0.000		Unlikely to be X-ray source
RXJ114621.27+285320.6	11 46 19.93	+28 53 06.6	cat	cluster	0.170	part of [VMF98] 107	
RXJ115952.10+553212.1	11 59 52.28	+55 32 06.1	cat	cluster	0.081	MS 1157.3+5548	
RXJ120403.79+280711.2	12 04 03.55	+28 07 01.3	cat	cluster	0.167	MS 1201.5+2824	
RXJ121017.25+391822.6	12 10 16.61	+39 18 16.6	ISIS	NELG	0.022		
RXJ121115.30+391146.8	12 11 15.67	+39 11 54.2	cat	cluster	0.340	MS 1208.7+3928	
RXJ121803.82+470854.6	12 18 4.54	+47 08 51.0	ISIS	BLAGN	1.743		
RXJ124913.86-055906.2	12 49 13.85	-05 59 19.4	cat	BLAGN	2.212	[HB89] 1246-057	BALQSO
RXJ131635.62+285942.7	13 16 34.72	+28 59 29.3	cat	BLAGN	0.277	RIXOS F224_026	
RXJ133146.37+111420.4	13 31 45.93	+11 14 12.8	ISIS	star	0.000		Unlikely to be X-ray source
RXJ133147.00+105653.0	13 31 46.58	+10 56 55.7	cat	star	0.000	RIXOS F278_026	
RXJ133152.51+111643.5	13 31 52.25	+11 16 49.6	cat	BLAGN	0.090	RIXOS F278_010	
RXJ135105.69+601538.5	13 51 06.33	+60 15 39.5	ISIS	NELG	0.291		
RXJ135529.59+182413.6	13 55 29.54	+18 24 21.3	cat	BLAGN	1.196	RIXOS F268_011	
RXJ140134.94+542029.2	14 01 34.59	+54 20 31.1	ISIS	galaxy	0.069		
RXJ140416.61+541618.2	14 04 16.79	+54 16 14.6	ISIS	BLAGN	1.405		
RXJ142754.71+330007.0	14 27 54.51	+32 59 59.8	cat	BLAGN	0.420	RIXOS F110_034	Uncertain ID
RXJ163054.25+781105.1	16 30 55.00	+78 11 03.9	cat	BLAGN	0.358		
RXJ163308.57+570258.7	16 33 08.59	+57 02 54.8	ISIS	BLAGN	2.802	WN B1632+5709	
RXJ170041.60+641259.0	17 00 41.71	+64 12 58.4	ISIS	cluster	0.230	ABELL 2246	
RXJ170123.32+641413.0	17 01 23.47	+64 14 11.8	cat	cluster	0.440	[RTH97] B	
RXJ204640.48-363147.5	20 46 40.13	-36 31 48.1	EFOSC	BLAGN	1.122		
RXJ204716.74-364715.1	20 47 16.75	-36 47 23.2	EFOSC	NELG	0.050		
RXJ213807.61-423614.3	21 38 07.97	-42 36 17.8	EFOSC	BLAGN	0.019	ESO 287- G 042	
RXJ223619.89-261426.2	22 36 20.43	-26 14 37.4	EFOSC	star	0.000		
RXJ235113.89+201347.3	23 51 13.91	+20 13 46.4	cat	NELG	0.043	MCG +03-60-031	

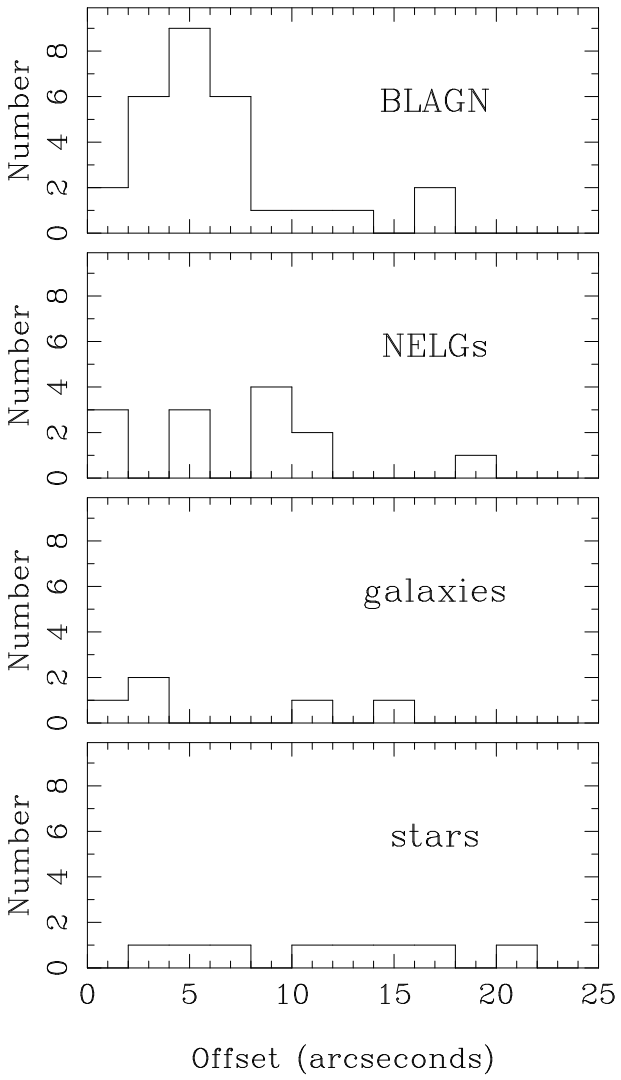

Figure 1. Histogram of offsets, in bins of 2 arcseconds, between the X–ray positions and optical counterparts for the different classes of identified sources.

Note that the very hard mean spectral index of the Galactic stars (see Table 2) is due to the three objects with best fit $\alpha < -1$, two of which (RXJ112056.87 +132726.2 with best fit $\alpha = -1.65$ and RXJ133146.37+111420.4 with best fit $\alpha = -1.472$) are unlikely to be correct identifications (see Section 3.6).

The other three types of sources (BLAGN, NELGs and galaxies) have distributions of (α, S) which are indistinguishable from one another according to the 2DKS test; any (or all) could be significant contributors to the faint, hard population.

For comparison Figure 2 also shows the unidentified sources. Unidentified objects in the spectroscopic sample are found with similar spectral slopes and fluxes to the identified sources (except the clusters which are softer and brighter). The sources in the imaging sample are more concentrated toward faint fluxes and comprise most of the faintest ($S \sim 10^{-14}$ erg cm^{-2} s^{-1}) hard sources.

3.2 The unidentified sources

We now consider briefly how fair a subsample the identified sources are of the whole *ROSAT* hard source sample. Starting with the spectroscopic sample, candidates were chosen for identification on our WHT and ESO 3.6m observing runs without regard to their optical magnitudes and morphologies, (except to exclude sources with an existing catalogue identification) and are hence an unbiased subsample of the spectroscopic sample. The catalogue identifications, although including a few optically bright galaxies, are mostly from previous flux limited X–ray surveys. They therefore tend to have higher X–ray fluxes than the spectroscopic sample as a whole, but are otherwise a fair subsample. This means that except for a bias towards higher X–ray fluxes, the identified sources are a fair subsample of the spectroscopic sample.

The spectroscopic sample is a significant fraction of the whole *ROSAT* hard source sample (103 of 147 sources), but it cannot be considered a fair subsample because it excludes the optically faint sources which form the imaging sample. Without spectroscopically identifying the imaging sample (which is currently impractical) it is not possible to determine whether or not the imaging sample is *actually* made up of the same mix of sources as the spectroscopic sample. However we can examine whether it is *possible*, by assuming that similar types of sources will have similar X–ray to optical flux ratios. Figure 3 shows the X–ray flux against the APM red (E or R) magnitude for the identified sources with available APM data. BLAGN, NELGs and galaxies are found with similar ranges of X–ray to optical ratio. The optical counterparts to the imaging sample sources are presumed to be fainter than the plate limit, which we take to be 20.5 and 21.0 for sources with APM data available for E and R plates respectively. The imaging sample sources are plotted in Fig. 3 with these lower limits except for two sources RXJ031956.76-663938.5 and RXJ101031.05+503458.6, which are in the imaging sample because there are too many potential counterparts for practical spectroscopic follow up. The dashed line corresponds to an X–ray to optical flux ratio which is similar to that of RXJ111750.51+075712.8, which has the highest X–ray to optical flux ratio of the identified spectroscopic sample sources excluding the clusters. Only six of the imaging sample sources lie above the dashed line, and therefore definitely have X–ray to optical flux ratios different to those of the identified sources. Therefore the limits on the optical to X–ray ratios are consistent with the identified sources being the same types of objects as constitute almost the whole *ROSAT* hard source sample.

3.3 Redshifts and luminosities

Fig. 4 shows the redshifts and 0.5 - 2 keV luminosities for the extragalactic hard sources. Luminosities were calculated from the fitted fluxes, K corrected using the best fit spectral slopes, and assuming $H_0 = 50$ km s^{-1} Mpc^{-3}, $q_0 = 0$. The majority of the BLAGN have higher luminosities and redshifts than the NELGs and galaxies; all the high redshift ($z > 1$) sources are BLAGN. This may imply that either hard spectrum narrow line sources do not exist at high luminosity/redshift or our spectroscopic

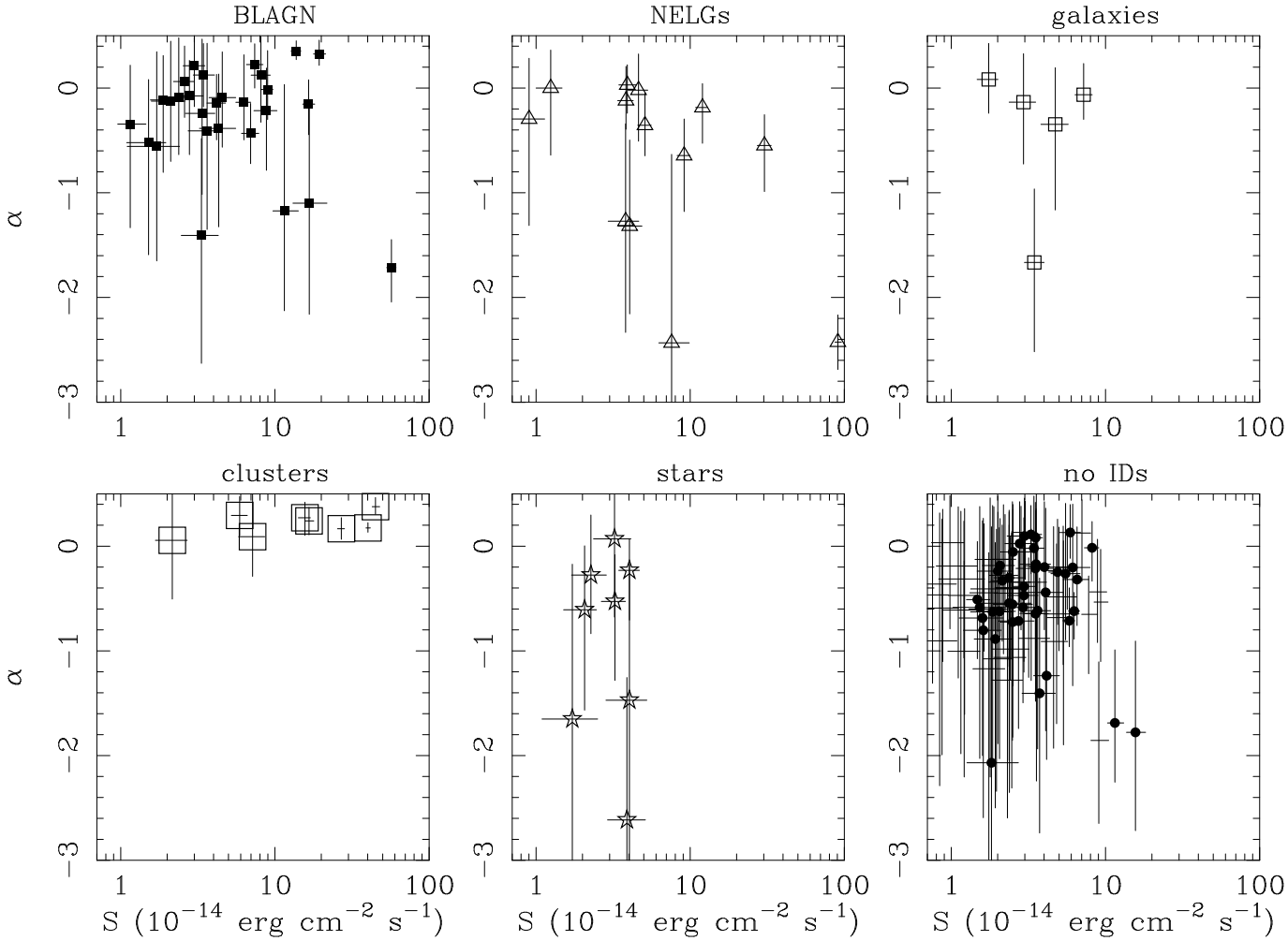

Figure 2. X-ray spectral slopes and fluxes of the different types of hard source. For comparison the unidentified sources are shown in the last panel: the spectroscopic sample as filled dots and the imaging sample as crosses (see Section 2 for definitions of the two samples).

sample is not deep enough (in X–ray or optical flux) to find them.

3.4 X–ray - optical - radio flux ratios

It is common to parameterise the X–ray to optical and optical to radio flux ratios of AGN as α_{OX} and α_{OR}, where α_{OX} is the slope of the power law which (in the object's rest frame) would connect the flux density (F_ν) at 2500 Å with the X–ray flux density at 2 keV, and α_{OR} is the slope of the power law which would connect the flux density at 2500 Å with the flux density at 5 GHz.

For all sources we have estimated the rest frame 2500 Å flux density using B photometry (taken from Carrera et al. in preparation) and assuming a power law optical - UV spectrum with slope $\alpha = 0.5$, and using the B magnitude to flux conversion given by Wilkes et al. (1994). The B magnitudes have been corrected for Galactic reddening using the expression for $E(B-V)$ in Bohlin, Savage & Drake (1978) and assuming $A_B = 4E(B_V)$.

To estimate the rest frame 5 GHz fluxes we have searched for potential radio counterparts to our X–ray sources in the catalogues of radio sources in the VLA 1.4 GHz FIRST (White et al. 1997) and NVSS (Condon et al. 1998) surveys and the 5 GHz Parkes-MIT-NRAO (PMN, Griffith & Wright 1993) survey. Additionally, radio images from these surveys were searched by eye to ensure that any extended radio sources associated with our X–ray sources were not missed, and to ensure that there were no spurious radio counterparts associated with other extended radio sources. The uncertainty in radio source position from these three surveys ranges from $\sim$ better than 1 arcsecond (FIRST) to around 10 arcseconds (PMN). The sky density of radio sources is sufficiently low (reaching around 100 deg^{-2} at the $\sim$1 mJy completeness limit of FIRST) that it is unlikely that there are any chance coincidences. Where no suitable radio source appears in a survey catalogue, we have taken the catalogue completeness limit as the upper limit to the radio flux of the X–ray source. We took the best measurement (or upper limit) available from the three surveys and assume a radio spectral slope of $\alpha = 0.7$.

The 2 keV flux density has been estimated from the

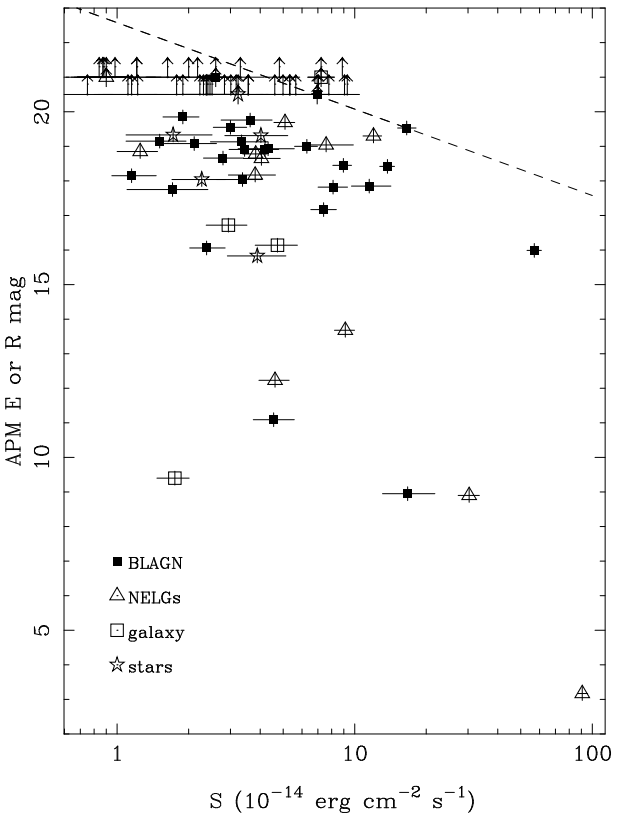

Figure 3. Optical magnitudes against X–ray fluxes for the identified sources inthe spectroscopic sample (symbols) and the sources in the imaging sample (lower limits). The gradient of the dashed line corresponds to a constant ratio of X–ray to optical flux.

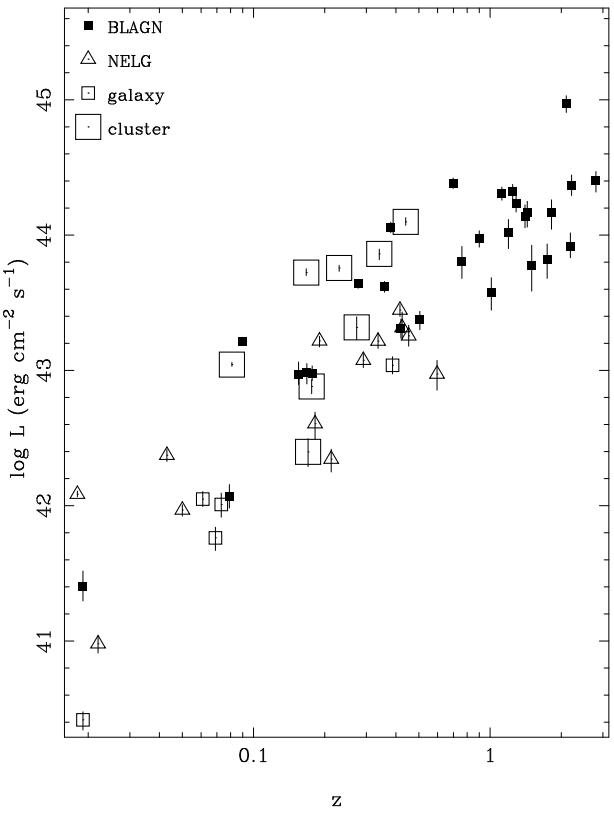

Figure 4. Redshifts and observed 0.5 - 2 keV luminosities for the different extragalactic source types

fitted 0.5 - 2 keV fluxes and assuming an X–ray spectral slope of $\alpha = 0$.

We then computed

$\alpha_{OX} = 0.384 \log[f_\nu(2500\text{Å})/f_\nu(2\text{keV})]$

and

$\alpha_{OR} = -0.186 \log[f_\nu(2500\text{Å})/f_\nu(5\text{GHz})]$

α_{OX} and α_{OR} are shown in Fig. 5 for all the hard sources identified as BLAGN, NELGs and galaxies. The horizontal dashed line marks $\alpha_{OR} = 0.35$ which is commonly used to differentiate radio loud and radio quiet objects (Zamorani et al. 1981). Seven hard sources (four BLAGN, 2 galaxies and 1 NELG) lie above this line, and are therefore radio loud. This is a large radio loud fraction (15^{+7}_{-5}% where errors are the Poission 68% confidence interval, Gehrels 1986) of the BLAGN, NELGs and galaxies compared to the fraction found in normal *ROSAT* surveys *without* spectral selection, eg Cilliegi et al. (1995) find that only two of the eighty CRSS AGN and NELGs ($2.5^{+3.3}_{-1.6}$%) are radio loud. On the other hand, the distribution of α_{OX} of the hard sources is quite similar to that found in other AGN surveys (eg Ciliegi et al. 1995, Wilkes et al. 1994), with the majority of sources having $1 < \alpha_{OX} < 1.8$.

3.5 X–ray absorption

The leading hypothesis to explain the majority of faint hard sources which contribute substantially to the XRB is that they are intrinsically absorbed AGN (eg Fabian & Iwasawa 1999, Setti & Woltjer 1989). This is also a likely hypothesis for our hard sources, because the optical spectra and colours of a significant fraction of our BLAGN and NELGs suggest absorption (Mittaz et al. 2001 and Carrera et al. 2001). Assuming that our BLAGN, NELGs and galaxies have hard spectra because of absorption, we have estimated their column densities from their 3 colour *ROSAT* PSPC spectra. We assume that before absorption they have power law X–ray spectra with energy index $\alpha = 1$ (typical for X-ray selected AGN, eg Mittaz et al. 1999, Maccacaro et al. 1988) and fit their intrinsic cold gas column. The fitting procedure was identical to that described in paper 1 except that the free parameters in the fit are intrinsic column and power law normalisation rather than power law slope and normalisation. The results of these fits are given in Table 3.

The BLAGN, NELG and galaxies' fitted absorbing columns and luminosities (before absorption) are shown in Fig. 6. Most of the high luminosity sources (near the top of Fig. 6) are BLAGN, while most of the galaxies are found with low luminosities; the mean log L (in erg s^{-1}, 0.5 - 2 keV) for the BLAGN, NELGs and galaxies are 44.4, 43.2 and 42.2 respectively. We note that the trend in Fig. 6 for the most absorbed sources to have the highest luminosity is probably a selection effect due to the shifting of the rest frame emitted passband to higher energy with increasing redshift. This means that sources detectable in the PSPC and satisfying our spectral selection criterion

Table 3. Hard source α_{OX}, α_{OR} and fitted columns

Source	X–ray flux[a]	X–ray α	X–ray log L[b]	B mag	A_B	radio flux (mJy)	radio ν (GHz)	radio survey	α_{OX}	α_{OR}	X–ray column fit N_H (cm^{-2})	X–ray column fit norm[c]
RXJ001144.43-362638.0	$4.19^{+0.60}_{-0.56}$	$-0.14^{+0.27}_{-0.35}$	$43.97^{+0.06}_{-0.06}$	20.38± 0.12	0.08	< 2.50	1.4	NVSS	$1.32^{+0.04}_{-0.04}$	< 0.33	$21.34^{+0.43}_{-0.29}$	$2.32^{+0.52}_{-0.39}$
RXJ004651.98-204329.0	$19.37^{+1.95}_{-1.56}$	$0.32^{+0.13}_{-0.11}$	$44.05^{+0.04}_{-0.04}$	18.60± 0.30	0.11	< 2.50	1.4	NVSS	$1.30^{+0.06}_{-0.06}$	< 0.21	$20.72^{+0.08}_{-0.09}$	$9.91^{+0.89}_{-0.92}$
RXJ005734.78-272827.4	$1.15^{+0.31}_{-0.20}$	$-0.34^{+0.56}_{-0.99}$	$43.91^{+0.10}_{-0.08}$	18.62± 0.16	0.13	< 2.50	1.4	NVSS	$1.84^{+0.06}_{-0.06}$	< 0.21	$22.60^{+0.26}_{-0.48}$	$0.90^{+0.33}_{-0.27}$
RXJ005736.81-273305.9	$1.25^{+0.23}_{-0.25}$	$0.00^{+0.36}_{-0.64}$	$42.34^{+0.07}_{-0.10}$	20.72± 0.30	0.13	< 2.50	1.4	NVSS	$1.42^{+0.08}_{-0.07}$	< 0.36	$21.07^{+0.40}_{-0.46}$	$0.79^{+0.22}_{-0.18}$
RXJ005746.75-273000.8	$1.75^{+0.26}_{-0.28}$	$0.08^{+0.34}_{-0.32}$	$40.42^{+0.06}_{-0.08}$	13.53± 0.10	0.13	3.80± 0.70	1.4	NVSS	$2.45^{+0.04}_{-0.04}$	$-0.16^{+0.02}_{-0.02}$	$20.80^{+0.29}_{-0.28}$	$1.02^{+0.21}_{-0.18}$
RXJ005801.64-275308.6	$5.09^{+0.50}_{-0.52}$	$-0.35^{+0.31}_{-0.29}$	$43.45^{+0.04}_{-0.05}$	21.43± 0.15	0.13	< 2.50	1.4	NVSS	$1.09^{+0.04}_{-0.04}$	< 0.41	$21.55^{+0.17}_{-0.25}$	$3.31^{+0.71}_{-0.54}$
RXJ005812.20-274217.8	$0.90^{+0.24}_{-0.22}$	$-0.30^{+0.58}_{-1.02}$	$42.97^{+0.10}_{-0.12}$	22.63± 0.30	0.13	< 2.50	1.4	NVSS	$1.21^{+0.09}_{-0.09}$	< 0.51	$21.75^{+0.29}_{-0.57}$	$0.65^{+0.29}_{-0.17}$
RXJ013721.47-182558.3	$3.91^{+0.57}_{-0.46}$	$0.03^{+0.19}_{-0.27}$	$43.22^{+0.06}_{-0.05}$	20.87± 0.11	0.07	< 2.50	1.4	NVSS	$1.23^{+0.04}_{-0.04}$	< 0.36	$20.84^{+0.17}_{-0.15}$	$2.02^{+0.30}_{-0.26}$
RXJ014159.22-543037.0	$8.81^{+1.51}_{-1.51}$	$-0.22^{+0.41}_{-0.57}$	$42.98^{+0.07}_{-0.08}$	17.38± 0.10	0.17	< 37.00	5.0	PMN	$1.60^{+0.05}_{-0.04}$	< 0.39	$21.37^{+0.20}_{-0.46}$	$5.98^{+1.77}_{-1.54}$
RXJ031456.58-552006.8	$3.45^{+0.54}_{-0.48}$	$-1.66^{+0.70}_{-0.85}$	$43.04^{+0.06}_{-0.06}$	21.72± 0.13	0.18	1.25± 0.11	1.4	FIRST	$1.10^{+0.05}_{-0.04}$	$0.37^{+0.02}_{-0.02}$	$22.12^{+0.10}_{-0.15}$	$4.42^{+1.18}_{-1.03}$
RXJ033340.22-391833.4	$3.37^{+0.70}_{-0.75}$	$-0.24^{+0.71}_{-0.77}$	$44.17^{+0.08}_{-0.11}$	19.42± 0.12	0.10	< 2.50	1.4	NVSS	$1.52^{+0.06}_{-0.05}$	< 0.26	$22.48^{+0.19}_{-0.37}$	$3.01^{+1.19}_{-0.97}$
RXJ033402.54-390048.7	$7.22^{+0.99}_{-0.87}$	$-0.06^{+0.30}_{-0.23}$	$42.05^{+0.06}_{-0.06}$	16.03± 0.30	0.10	1567.10± 52.60	1.4	NVSS	$1.84^{+0.07}_{-0.07}$	$0.51^{+0.03}_{-0.03}$	$20.74^{+0.29}_{-0.22}$	$3.97^{+0.69}_{-0.58}$
RXJ034119.02-441033.3	$2.60^{+0.41}_{-0.40}$	$0.06^{+0.34}_{-0.34}$	$43.37^{+0.06}_{-0.07}$	21.55± 0.11	0.10	< 45.00	5.0	PMN	$1.19^{+0.04}_{-0.04}$	< 0.72	$21.10^{+0.38}_{-0.31}$	$1.48^{+0.34}_{-0.25}$
RXJ043420.48-082136.7	$11.51^{+2.69}_{-1.82}$	$-1.17^{+1.21}_{-0.95}$	$42.97^{+0.09}_{-0.07}$	18.68± 0.13	0.42	3.70± 0.60	1.4	NVSS	$1.32^{+0.05}_{-0.05}$	$0.24^{+0.02}_{-0.02}$	$21.95^{+0.11}_{-0.22}$	$14.67^{+5.80}_{-4.18}$
RXJ045558.99-753229.1	$90.78^{+4.93}_{-3.88}$	$-2.43^{+0.26}_{-0.26}$	$42.08^{+0.02}_{-0.02}$	16.05± 0.07	0.59	< 20.00	5.0	PMN	$1.34^{+0.02}_{-0.02}$	< 0.27	$21.89^{+0.04}_{-0.04}$	$135.47^{+13.96}_{-12.08}$
RXJ082640.20+263112.3	$3.81^{+0.83}_{-0.87}$	$-1.27^{+0.93}_{-1.06}$	$42.61^{+0.09}_{-0.11}$	20.34± 0.14	0.25	< 0.91	1.4	FIRST	$1.27^{+0.06}_{-0.05}$	< 0.25	$21.93^{+0.15}_{-0.22}$	$4.57^{+2.06}_{-1.38}$
RXJ085340.52+134924.9	$12.00^{+0.98}_{-1.16}$	$-0.19^{+0.23}_{-0.34}$	$43.22^{+0.03}_{-0.04}$	19.21± 0.09	0.25	23.20± 1.50	1.4	NVSS	$1.26^{+0.03}_{-0.03}$	$0.42^{+0.01}_{-0.01}$	$21.38^{+0.15}_{-0.25}$	$7.80^{+1.52}_{-1.22}$
RXJ085851.49+141150.7	$4.05^{+0.81}_{-0.65}$	$-1.32^{+0.82}_{-0.84}$	$43.26^{+0.08}_{-0.08}$	20.82± 0.30	0.29	< 2.50	1.4	NVSS	$1.20^{+0.08}_{-0.08}$	< 0.39	$22.11^{+0.13}_{-0.18}$	$4.81^{+1.51}_{-1.37}$
RXJ090518.27+335006.0	$7.58^{+2.29}_{-1.33}$	$-2.43^{+1.80}_{-1.09}$	$43.32^{+0.11}_{-0.08}$	20.45± 0.09	0.16	< 0.97	1.4	FIRST	$1.17^{+0.05}_{-0.06}$	< 0.25	$22.41^{+0.08}_{-0.18}$	$15.65^{+6.87}_{-4.00}$
RXJ090923.64+423629.2	$7.40^{+0.97}_{-0.87}$	$0.22^{+0.20}_{-0.22}$	$42.98^{+0.05}_{-0.05}$	18.25± 0.09	0.11	< 2.50	1.4	NVSS	$1.50^{+0.04}_{-0.03}$	< 0.16	$20.69^{+0.17}_{-0.18}$	$3.86^{+0.51}_{-0.50}$
RXJ091908.27+745305.6	$4.73^{+1.01}_{-0.92}$	$-0.35^{+0.54}_{-0.82}$	$42.01^{+0.08}_{-0.09}$	17.82± 0.09	0.14	< 2.50	1.4	NVSS	$1.63^{+0.05}_{-0.05}$	< 0.13	$21.57^{+0.27}_{-0.42}$	$4.01^{+2.69}_{-1.61}$
RXJ094144.51+385434.8	$2.11^{+0.51}_{-0.53}$	$-0.12^{+0.57}_{-0.58}$	$44.17^{+0.09}_{-0.13}$	21.11± 0.14	0.10	< 1.01	1.4	FIRST	$1.35^{+0.07}_{-0.06}$	< 0.32	$21.92^{+0.46}_{-0.43}$	$1.34^{+0.41}_{-0.37}$
RXJ095340.67+074426.1	$4.32^{+1.25}_{-1.09}$	$-0.38^{+0.52}_{-0.94}$	$43.81^{+0.11}_{-0.13}$	20.01± 0.09	0.19	< 2.50	1.4	NVSS	$1.35^{+0.06}_{-0.06}$	< 0.31	$21.77^{+0.34}_{-0.45}$	$3.06^{+1.44}_{-0.95}$
RXJ101112.05+554451.3	$6.95^{+0.90}_{-0.88}$	$-0.43^{+0.29}_{-0.29}$	$44.32^{+0.05}_{-0.06}$	22.02± 1.00	0.05	161.50± 0.15	1.4	FIRST	$1.00^{+0.18}_{-0.17}$	$0.78^{+0.07}_{-0.07}$	$21.62^{+0.43}_{-0.17}$	$4.01^{+0.91}_{-0.57}$
RXJ101123.17+524912.4	$3.34^{+0.96}_{-0.87}$	$-1.41^{+0.93}_{-1.22}$	$43.58^{+0.11}_{-0.13}$	20.86± 0.09	0.05	< 0.96	1.4	FIRST	$1.29^{+0.06}_{-0.06}$	< 0.28	$22.51^{+0.16}_{-0.28}$	$3.91^{+1.96}_{-1.21}$
RXJ101147.48+505002.2	$4.56^{+1.01}_{-0.82}$	$-0.09^{+0.44}_{-0.47}$	$42.07^{+0.09}_{-0.09}$	16.74± 0.22	0.06	< 0.96	1.4	FIRST	$1.82^{+0.07}_{-0.07}$	< -0.02	$20.65^{+0.73}_{-0.28}$	$2.75^{+0.95}_{-0.55}$
RXJ104723.37+540412.6	$1.71^{+0.70}_{-0.61}$	$-0.56^{+0.90}_{-1.09}$	$43.78^{+0.15}_{-0.19}$	20.09± 0.11	0.06	< 0.96	1.4	FIRST	$1.54^{+0.09}_{-0.07}$	< 0.23	$22.22^{+0.42}_{-0.61}$	$1.31^{+0.78}_{-0.45}$
RXJ110742.05+723236.0	$8.11^{+1.22}_{-1.10}$	$0.12^{+0.37}_{-0.45}$	$44.97^{+0.06}_{-0.06}$	19.07± 0.08	0.21	370.60± 11.10	1.4	NVSS	$1.43^{+0.04}_{-0.04}$	$0.64^{+0.01}_{-0.01}$	$21.58^{+0.82}_{-0.38}$	$4.75^{+1.11}_{-0.75}$
RXJ111750.51+075712.8	$16.55^{+1.57}_{-1.40}$	$-0.15^{+0.23}_{-0.29}$	$44.38^{+0.04}_{-0.04}$	20.67± 0.09	0.24	< 2.50	1.4	NVSS	$1.01^{+0.03}_{-0.03}$	< 0.36	$21.57^{+0.18}_{-0.20}$	$9.94^{+1.60}_{-1.26}$
RXJ111942.16+211518.1	$3.44^{+0.62}_{-0.48}$	$0.13^{+0.30}_{-0.30}$	$44.24^{+0.07}_{-0.07}$	19.91± 0.09	0.09	< 0.93	1.4	FIRST	$1.44^{+0.04}_{-0.04}$	< 0.21	$21.42^{+0.36}_{-0.28}$	$1.89^{+0.37}_{-0.30}$
RXJ121017.25+391822.6	$4.62^{+0.68}_{-0.67}$	$-0.02^{+0.35}_{-0.49}$	$40.98^{+0.06}_{-0.07}$	17.18± 0.50	0.14	< 0.98	1.4	FIRST	$1.73^{+0.10}_{-0.10}$	< 0.04	$21.10^{+0.22}_{-0.49}$	$2.88^{+0.78}_{-0.51}$
RXJ121803.82+470854.6	$1.51^{+0.44}_{-0.42}$	$-0.52^{+0.60}_{-1.07}$	$43.82^{+0.11}_{-0.14}$	21.04± 0.09	0.08	< 0.98	1.4	FIRST	$1.42^{+0.07}_{-0.06}$	< 0.31	$22.30^{+0.34}_{-0.69}$	$1.07^{+0.53}_{-0.30}$
RXJ124913.86-055906.2	$2.38^{+0.47}_{-0.36}$	$-0.09^{+0.57}_{-0.55}$	$44.36^{+0.08}_{-0.07}$	17.26± 0.30	0.15	< 2.50	1.4	NVSS	$1.92^{+0.07}_{-0.08}$	< 0.12	$22.23^{+0.36}_{-0.57}$	$1.53^{+0.39}_{-0.38}$
RXJ131635.62+285942.7	$13.74^{+0.98}_{-1.00}$	$0.35^{+0.10}_{-0.08}$	$43.64^{+0.03}_{-0.03}$	20.32± 0.30	0.08	< 0.93	1.4	FIRST	$1.10^{+0.06}_{-0.06}$	< 0.25	$20.53^{+0.07}_{-0.07}$	$6.55^{+0.50}_{-0.47}$
RXJ133152.51+111643.5	$56.99^{+4.09}_{-3.88}$	$-1.72^{+0.27}_{-0.33}$	$43.22^{+0.03}_{-0.03}$	18.16± 0.10	0.13	8.00± 1.00	1.4	NVSS	$1.17^{+0.03}_{-0.03}$	$0.24^{+0.02}_{-0.02}$	$21.80^{+0.06}_{-0.06}$	$64.44^{+9.09}_{-7.69}$
RXJ135105.69+601538.5	$3.83^{+0.44}_{-0.45}$	$-0.12^{+0.33}_{-0.27}$	$43.07^{+0.05}_{-0.05}$	20.53± 0.09	0.12	< 2.50	1.4	NVSS	$1.27^{+0.03}_{-0.03}$	< 0.33	$21.17^{+0.23}_{-0.25}$	$2.22^{+0.42}_{-0.31}$
RXJ135529.59+182413.6	$3.63^{+0.86}_{-0.89}$	$-0.41^{+0.84}_{-0.94}$	$44.02^{+0.09}_{-0.12}$	20.61± 0.09	0.14	< 2.50	1.4	NVSS	$1.31^{+0.06}_{-0.05}$	< 0.35	$22.25^{+0.25}_{-0.50}$	$2.82^{+1.29}_{-0.78}$
RXJ140134.94+542029.2	$2.94^{+0.58}_{-0.57}$	$-0.13^{+0.46}_{-0.59}$	$41.76^{+0.08}_{-0.09}$	18.42± 0.09	0.08	< 1.00	1.4	FIRST	$1.63^{+0.05}_{-0.04}$	< 0.10	$21.02^{+0.39}_{-0.46}$	$1.89^{+0.64}_{-0.39}$
RXJ140416.61+541618.2	$2.79^{+0.62}_{-0.48}$	$-0.08^{+0.34}_{-0.56}$	$44.14^{+0.09}_{-0.08}$	21.16± 0.20	0.08	< 0.99	1.4	FIRST	$1.28^{+0.06}_{-0.06}$	< 0.32	$21.69^{+0.40}_{-0.38}$	$1.70^{+0.45}_{-0.35}$
RXJ142754.71+330007.0	$3.00^{+0.51}_{-0.46}$	$0.21^{+0.27}_{-0.39}$	$43.31^{+0.07}_{-0.07}$	19.66± 0.08	0.07	< 0.83	1.4	FIRST	$1.46^{+0.04}_{-0.04}$	< 0.18	$20.81^{+0.38}_{-0.35}$	$1.57^{+0.29}_{-0.27}$
RXJ163054.25+781105.1	$8.96^{+0.74}_{-0.87}$	$-0.01^{+0.37}_{-0.29}$	$43.62^{+0.03}_{-0.04}$	20.54± 0.14	0.28	< 2.50	1.4	NVSS	$1.11^{+0.04}_{-0.04}$	< 0.35	$21.52^{+0.17}_{-0.31}$	$5.81^{+1.22}_{-1.06}$
RXJ163308.57+570258.7	$1.89^{+0.32}_{-0.33}$	$-0.11^{+0.42}_{-0.69}$	$44.40^{+0.07}_{-0.08}$	20.06± 0.12	0.13	17.20± 0.15	1.4	FIRST	$1.55^{+0.05}_{-0.04}$	$0.47^{+0.01}_{-0.01}$	$22.48^{+0.31}_{-0.54}$	$1.20^{+0.33}_{-0.26}$
RXJ204640.48-363147.5	$6.29^{+0.68}_{-0.71}$	$-0.14^{+0.45}_{-0.36}$	$44.31^{+0.04}_{-0.05}$	18.76± 0.07	0.28	23.70± 0.90	1.4	NVSS	$1.48^{+0.03}_{-0.03}$	$0.40^{+0.01}_{-0.01}$	$21.89^{+0.17}_{-0.22}$	$3.92^{+0.65}_{-0.57}$
RXJ204716.74-364715.1	$9.13^{+0.86}_{-0.91}$	$-0.64^{+0.35}_{-0.53}$	$41.97^{+0.04}_{-0.05}$	17.57± 0.08	0.28	4.60± 0.50	1.4	NVSS	$1.54^{+0.03}_{-0.03}$	$0.16^{+0.01}_{-0.01}$	$21.53^{+0.12}_{-0.15}$	$7.88^{+1.65}_{-1.37}$
RXJ213807.61-423614.3	$16.71^{+5.05}_{-3.62}$	$-1.10^{+0.92}_{-1.06}$	$41.40^{+0.11}_{-0.11}$	16.15± 0.07	0.18	< 47.00	5.0	PMN	$1.67^{+0.05}_{-0.05}$	< 0.32	$21.74^{+0.17}_{-0.27}$	$19.00^{+9.30}_{-6.98}$
RXJ235113.89+201347.3	$30.31^{+3.16}_{-3.06}$	$-0.55^{+0.29}_{-0.44}$	$42.37^{+0.04}_{-0.05}$	16.94± 0.13	0.30	5.90± 0.50	1.4	NVSS	$1.43^{+0.04}_{-0.04}$	$0.14^{+0.02}_{-0.02}$	$21.44^{+0.12}_{-0.18}$	$23.84^{+5.35}_{-4.08}$

[a] Units of erg cm^{-2} s^{-1}
[b] See Section 3.3
[c] Units of erg cm^{-2} s^{-1} keV^{-1}

(see paper 1) will have larger columns at higher redshift (and hence at higher luminosity).

3.6 Notes on individual sources

RXJ004651.98-204329.0 The hard *ROSAT* spectrum of this active galaxy was the subject of Elvis et al. (1997) who proposed that absorption in material associated with NGC247 may be responsible.

RXJ005801.64-275308.6 A second, slightly fainter NELG at J2000 position $00^h58^m1.69^s - 27^\circ53'16.80''$ has the same redshift (z= 0.086) as, and is within 10 arcseconds of, the NELG identified as the X–ray source.

RXJ013707.63-183846.4 The star has an unremarkable G type spectrum, and the X–ray source is coincident with a bright radio source (MRC 0134-188) and hence the star is unlikely to be the correct optical counterpart. The real optical counterpart is too faint to be seen on POSS.

RXJ031456.58-552006.8 This radio galaxy has extended double lobe structure; see Gruppioni, Mignoli & Zamorani (1999).

RXJ033402.54-390048.7 This source is a wide angle

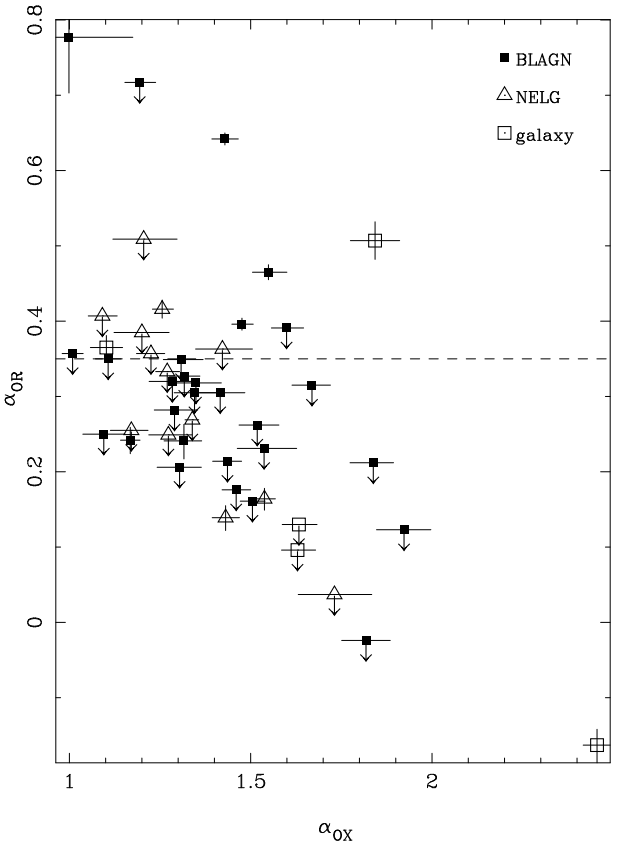

Figure 5. α_{OX} and α_{OR} for the hard sources

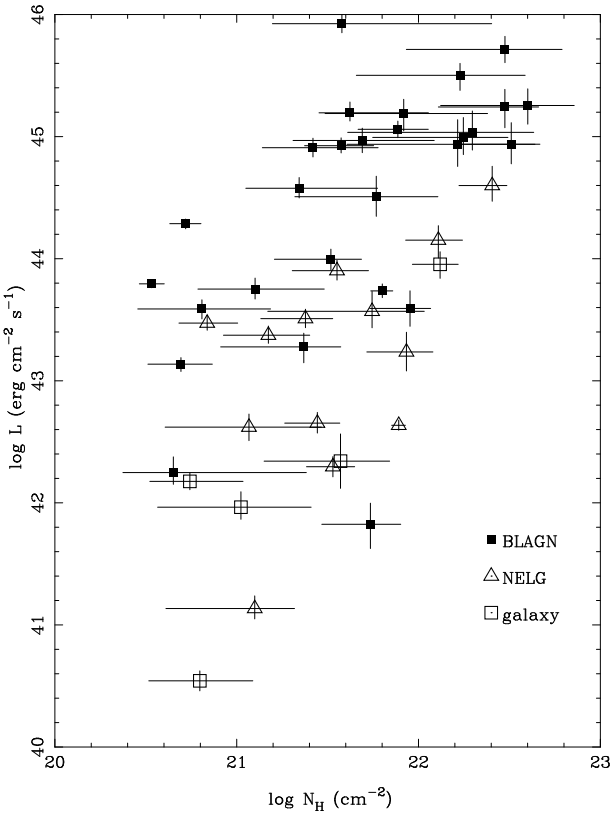

Figure 6. Fitted columns and unabsorbed 0.5-2 keV luminosities for the different types of hard sources.

tail radio source in the galaxy cluster Abell 3135. A magnitude V∼16 Galactic star is also close to the X-ray source position but is unlikely to be related.

RXJ043420.48-082136.7 The identification spectrum of this object was taken on the WHT as part of RIXOS, but the source was not part of the final RIXOS sample and is not included in the final catalogue (Mason et al. 2000).

RXJ085340.52+134924.9 This RIXOS identification is uncertain because there is another optical counterpart closer to the centre of the X–ray error circle that was not observed. Note also that the position of the optical counterpart is incorrect in Mason et al. (2000), which should be the same as that in Table 1, i.e. $08^h53^m41.01^s + 13^\circ49'19.7''$ (J2000).

RXJ095340.67+074426.1 The RIXOS identification and redshift of this source are based on a relatively poor optical spectrum and therefore may be incorrect.

RXJ101112.05+554451.3 This source was identified as an obscured radio loud AGN by Barcons et al. (1998). It has strong narrow emission lines but Mg II λ2798 is broad, and hence we have classified it as a BLAGN.

RXJ101147.48+505002.2 This X–ray source was identified with a NELG with $z = 0.067$ by Carballo et al. (1995), but we identify the source with a BLAGN with $z = 0.079$, which is brighter and closer to the X–ray source. Notably, the $z = 0.079$ BLAGN showed only narrow lines in the optical spectrum of Carballo et al. (1995); the Hα line profile appears genuinely to have changed between 1994 and 1998.

RXJ111926.34+210646.1 This galaxy cluster and the target of the PSPC observation (PG 1116+215) in which it was found have very similar redshifts (0.0176 and 0.1765 respectively) and therefore this source is not strictly serendipitous.

RXJ112056.87+132726.2 The X–ray source is coincident with the symmetric double radio source 87GB 111822.7+134349, and hence the star is unlikely to be the correct identification for the X–ray source.

RXJ120403.79+280711.2 This galaxy cluster and the target of the PSPC observation (PG 1202+281) in which it was found have similar redshifts (0.0167 and 0.1653 respectively) and therefore this source may not be strictly serendipitous.

RXJ124913.86-055906.2 This broad absorption line (BAL) QSO was the only bona-fide BALQSO in sample of Green & Mathur (1996) to be detected as a PSPC source.

RXJ133146.37+111420.4 This X–ray source is coincident with the radio source 87GB 132918.1+112918, and hence the star is unlikely to be the correct optical counterpart.

RXJ142754.71+330007.0 The RIXOS identification and redshift of this source are based on a relatively poor optical spectrum and therefore may be incorrect.

4 DISCUSSION

Excluding the clusters, which are unlikely to be an important part of the faint, hard X–ray source population (see

Section 3.1), we have identified 3 types of extragalactic hard source: BLAGN, NELGs and galaxies. At first sight the identification content of the sample appears similar to that of other PSPC surveys with similar flux limits but without any spectral selection, eg BLAGN being the most numerous source. However, in two respects the identification content of this survey is significantly different.

The first difference is that there is a higher proportion of radio loud objects (15^{+7}_{-5}%) in this survey (see Section 3.4). There are two possible reasons why this should be so. One is that the intrinsic X–ray emission of radio loud sources may be harder than that of radio quiet sources (Reeves et al. 1997) because the radio loud sources have an additional, hard spectrum X–ray emission component from the inner parts of radio jets. The other possibility is that our radio loud sources are absorbed, and because they are intrinsically more X–ray luminous than radio quiet sources they are relatively numerous in a relatively bright survey of hard spectrum sources. This would be analogous to the high proportion of (presumably unabsorbed) radio loud sources present in bright soft X–ray surveys (eg 11±2% in the EMSS, Della Ceca et al. 1994) compared to fainter soft X–ray surveys (eg $2.5^{+3.3}_{-1.6}$% in the CRSS, Ciliegi et al. 1995).

The second difference is that there are nearly half as many NELGs as BLAGN (see Table 1) compared to ratios of $\sim$ 1:13 NELGS to AGN in RIXOS (Mason et al. 2000) and $\sim$ 1:6 in the CCRS (Boyle, Wilkes & Elvis 1997). This implies that the fraction of sources with hard spectra is larger in the NELG population than in the BLAGN population. This is consistent with the findings that the NELGs in faint X–ray surveys have, on average, harder X–ray spectra than BLAGN (Romero-Colmenero et al. 1996, Almaini et al. 1996), and with the hypothesis that most X–ray selected NELGs are absorbed AGN (Schmidt et al. 1998, Lehmann et al. 2000).

Hence the hypothesis that most of the sources have hard X–ray spectra because they are absorbed could account for both the high radio loud and NELG content of this survey. It is also consistent with the preliminary analyses of the optical spectra and optical colours of the hard sources (Mittaz et al. 2001 and Carrera et al. 2001).

Related to the absorption hypothesis, an important finding is that the distributions of X–ray spectral slopes and fluxes of the BLAGN, NELGs and galaxies are indistinguishable within the current sample, but the three groups have different ranges of luminosities. The galaxies are found at low luminosity while the high luminosity sources are BLAGN (see figures 4 and 6). The absence of high luminosity, absorbed narrow line AGN has also been noted by Akiyama et al. (2000) in the *ASCA* Large Sky survey. These results are consistent with all three source types having the same mechanism for their X–ray spectra (an absorbed active nucleus) but optical emission line properties which depend on luminosity. For this reason we point out that the high redshift, high luminosity, absorbed QSOs expected to produce a large fraction of the X–ray background are not neccessarily narrow line objects (the proposed "QSO 2s") like Seyfert 2s, their low luminosity counterparts.

5 CONCLUSIONS

We have performed a survey of *ROSAT* fields for serendipitous sources with hard spectra ($\alpha < 0.5$); such sources must be a major contributor to the X–ray background at faint fluxes. In this paper we have presented optical identifications for 62 of these sources. Almost half (28) of these sources are BLAGN, while 12 are NELGs and 5 are galaxies without visible emission lines. We have also found 8 clusters of galaxies among the hard spectrum sources. However, these are predominantly bright sources and are not particularly hard (their best fit spectral indices all lie in the range $0.0 < \alpha < 0.5$), and hence clusters are unlikely to be an important component of the hard, faint population.

The hard spectrum BLAGN have a distribution of X–ray to optical ratios which is similar to that found for AGN from other soft X–ray surveys ($1 < \alpha_{OX} < 2$). However, a relatively large proportion (15%) of the BLAGN, NELGs and galaxies are radio loud. This could be because the radio jets in these objects produce intrinsically hard X–ray emission, or if they are absorbed, it could be because radio loud objects are more X–ray luminous than radio quiet objects.

The BLAGN, NELGs and galaxies have indistinguishable distributions of X–ray flux and spectra, hence any or all may be important to the hard, faint population required to solve the XRB spectral paradox. The majority of the galaxies are low luminosity sources, while the highest luminosity objects, and all the high redshift ($z > 1$) sources, are BLAGN. Their *ROSAT* spectra are consistent with their being AGN obscured by columns of $20.5 < \log(N_H/\mathrm{cm}^{-2}) < 23$. Overall, our data are consistent with the X–ray emission of the BLAGN, NELGs, and the galaxy sources coming from absorbed active nuclei.

6 ACKNOWLEDGMENTS

FJC thanks the DGES for partial financial support, under project PB95-0122. This research was based on observations collected at the European Southern Observatory, Chile, ESO No. 62.O-0659, and on observations made at the William Herschel Telescope which is operated on the island of La Palma by the Isaac Newton Group in the Spanish Observatorio del Roque de los Muchachos of the Instituto de Astrofisica de Canarias. This research has made use of data obtained from the Leicester Database and Archive Service at the Department of Physics and Astronomy, Leicester University, UK. This research has made use of the SIMBAD database, operated at CDS, Strasbourg, France, and of the NASA/IPAC Extragalactic Database (NED) which is operated by the Jet Propulsion Laboratory, California Institute of Technology, under contract with the National Aeronautics and Space Administration.

7 REFERENCES

Akiyama M., et al. , 2000, ApJ, in press (astro-ph/0001289)

Almaini O., Shanks T., Boyle B.J., Griffiths R.E., Roche

N., Stewart G.C., Georgantopoulos I., 1996, MNRAS, 282, 295
Barcons X., Carballo R., Ceballos M.T., Warwick R.S., Gonzalez-Serrano, 1998, MNRAS, 301, L25
Bohlin R.C., Savage B.D., Drake J.F., 1978, ApJ, 224, 132
Boyle B.J., Wilkes B.J. & Elvis M., 1997, MNRAS, 285, 511
Carballo R., et al. , 1995, MNRAS, 277, 1312
Carrera F.J., Mittaz J.P.D., Page M.J., 2001, proceedings of "X–ray astronomy '999: Stellar Endpoints, AGN and the Diffuse Background", eds G. Malaguti, G. Palumbo & N. White, in press
Ciliegi P., Elvis M., Wilkes B.J., Boyle B.J., McMahon R.G., Maccacaro T., 1995, MNRAS, 277, 1463
Condon J.J., Cotton W.D., Greisen E.W., Yin Q.F., Perley R.A., Taylor G.B., & Broderick J.J., 1998, AJ, 115, 1693
Della Ceca R., Zamorani G., Maccacaro T., Wolter A., Griffiths R., Stocke J.T., Setti G., 1994, ApJ, 430, 533
Elvis M., Fiore F., Giommi P., & Padovani P., 1997, MNRAS, 291, L49
Fabian A.C., 1999, MNRAS in press
Fabian A.C., Iwasawa K., 1999, MNRAS, 303, L34
Gehrels N., 1986, ApJ, 303, 336
Gilli R., Risaliti G., & Salvati M., 1999, A&A, 347, 424
Goodrich R.W., 1989, ApJ, 342, 224
Griffith M.R. & Wright A.E., 1993, AJ, 105, 1666
Gruppioni C., Mignoli M., & Zamorani G., 1999, MNRAS, 304, 199
Lehmann I., et al. , 2000, A&A, in press
Maccacaro T., Gioia I.M., Wolter A., Zamorani G., Stocke J.T., 1988, ApJ, 326, 680
Mason K.O., et al. , 2000, MNRAS, 311, 456
McHardy I.M., et al. , 1998, MNRAS, 295, 641
Mittaz J.P.D., Page M.J., Carrera F.J., 2001, proceedings of "X–ray astronomy '999: Stellar Endpoints, AGN and the Diffuse Background", eds G. Malaguti, G. Palumbo & N. White, in press
Mittaz et al. , 1999, MNRAS, 308, 233
Page M.J., Mittaz J.P.D. & Carrera F.J., 2000, 'paper 1', MNRAS, 318, 1073
Reeves, J. N., Turner M.J.L., Ohashi T., Kii T., 1997, MNRAS, 292, 468
Romero Colmenero E., Branduardi-Raymont G., Carrera F.J., Jones L.R., Mason K.O., McHardy I.M., Mittaz J.P.D., 1996, MNRAS, 282, 94
Schmidt M., Hasinger G., Gunn J., Schneider D., Burg R., Giacconi R., Lehmann I., MacKenty J., Trümper J., Zamorani G., 1998, A&A, 329, 495
Setti G., Woltjer L., 1989, A&A, 224, L21
White R.L., Becker R.H., Helfand D.J., & Gregg M.D., 1997, ApJ, 475, 479
Wilkes B.J., et al. 1994, ApJS, 92, 53
Zamorani G., et al. 1981, ApJ, 245, 357